Acoust. Sci. & Tech. **30**, 2 (2009)

PAPER

On the *in situ* estimation of surface acoustic impedance in interiors of arbitrary shape by acoustical inverse methods

Gabriel Pablo Nava[1,2,*], Yosuke Yasuda[3,†], Yoichi Sato[1,‡] and Shinichi Sakamoto[1,§]

[1]*Institute of Industrial Science, The University of Tokyo, Komaba 4–6–1, Meguro-ku, Tokyo, 153–8505 Japan*
[2]*NTT Communication Science Laboratories, NTT Co. Hikaridai 2–4, Seika-cho, Keihana Science City, Kyoto 619–0237 Japan*
[3]*Graduate School of Frontier Sciences, The University of Tokyo, Kashiwanoha 5–1–5, Kashiwa, 277–8563 Japan*

(*Received 14 December 2007, Accepted for publication 13 August 2008*)

Abstract: A method for *in situ* estimation of the acoustic impedance of surfaces in interiors is introduced in this paper. The key difference with traditional *in situ* measurement techniques is the use of an inverse acoustic boundary framework which allows us to overcome some geometry constraints from previous methods (such as the planar-surface requirement and placement of microphone arrays). Furthermore, estimation of the acoustic impedance of not only one but all the surfaces is possible provided that local reaction is the predominant effect, and the following parameters are known: geometry of the surfaces, sound pressure at a number of arbitrary points in the interior field and the strength of the sound source. The estimation of the acoustic impedance at each surface is achieved by the solution of an optimization problem formulated from the linear equations of the boundary element method (BEM) applied to the discretized interior boundaries of an interior space. Previous work on similar methods have reported examples with numerical simulations. The work in this paper goes further and numerical examples together with results obtained with experimental data are presented.

Keywords: *In-situ* measurement, Inverse boundary element method, Iterative optimization

PACS number: 43.55.Mc, 43.58.Fm [doi:10.1250/ast.30.100]

1. INTRODUCTION

Since around seven decades ago, several techniques for the measurement of sound absorption and acoustic impedance of the materials have been proposed [1]. Among them, laboratory methods (e.g. reverberation room and impedance tube) are extensively used providing important information about the test materials during an acoustic design stage. These methods, however, rely on assumptions of ideal acoustic conditions that in practice are not frequently met. For this reason, several *in situ* measurement techniques were developed. For example, one of the most widely used basic principles for *in situ* measurements is based on the use of two microphones to measure the direct and reflected sound over a planar test surface (e.g. [2–4]). In this approach the reflection coefficient is computed from the amplitude and phase relationships between the sound from the source and the reflected sound. While this technique is accurate at high frequencies, it will fail if unwanted reflections from other surfaces cannot be removed, or if non-plane wave reflections are predominant. These conditions are translated into geometrical constraints such as: *a*) the measurements should be performed in free field, or at least in a large space where the unwanted reflective surfaces are far enough, *b*) the test surface should be large, otherwise the accuracy at low frequency is poor, *c*) the microphones should be apart from the test surface so as to provide suitable measurement of the direct and reflected sound, but close enough so that undesired reflections can be clustered.

In efforts to overcome some of the above constraints, a method that uses a particle velocity and a sound pressure sensors integrated in a single package (named "microflown") has been developed [5]. By measuring the particle velocity and the sound pressure placing the microflown close to the test surface, the acoustic impedance of the normal and oblique incidence is calculated. Therefore, what this technique actually measures is the acoustic

*e-mail: pablo@cslab.kecl.ntt.co.jp
†e-mail: yyasuda@k.u-tokyo.ac.jp
‡e-mail: ysato@iis.u-tokyo.ac.jp
§e-mail: sakamoto@iis.u-tokyo.ac.jp

impedance of the incident wave at the near vicinity of the surface. Moreover, before performing the measurements, the microflown, together with the sound source, has to be calibrated either in a standing wave tube or in free field.

Another technique reported in [6] uses the sound of the surrounding ambient as source, hence eliminating the need of a speaker, and consequently the microphone-speaker calibration. In this approach the complex acoustic impedance of planar surfaces is estimated from the transfer functions of a pair of microphones collocated at prescribed distances from the test surface. Although this method is claimed to be universally applicable [6], a key step in the estimation of the transfer functions is to average the measured data over time and angle of incidence, which in turn implicitly imposes a strong assumption of random incidence of plane waves in a diffuse field (with almost no directivity), condition which in practical situations is hardly achieved.

In contrast to the traditional methods discussed above, a method which is applicable to arbitrary-shape surfaces is described in the following paragraphs. To estimate the normal-incidence acoustic impedance of all the surfaces within a room, the proposed algorithm takes as input: 1) the geometric model of the room, 2) the position and strength of a harmonically vibrating sound source, and 3) a set of sound pressures measured at arbitrary points in the interior field using a single microphone. The estimation of the acoustic impedance of the surfaces is formulated as an inverse boundary problem in which the boundary values of a bounded homogeneous domain are to be found from samples of the interior field governed by a wave propagation model. Similar acoustical inverse approaches have been studied before to localize and estimate the vibration strength on the surface of vibrating objects. The near-field acoustic holography (NAH) is the most representative technique in this context (e.g. [7–9]). On the other hand, scarce work in this context has been done for the *in situ* measurement of acoustic impedance. Nevertheless, one of the firsts attempts to estimate the acoustic impedance of interior surfaces was reported in [10], where the inverse formulation of the boundary problem is based on the finite element mehtod (FEM) framework in combination with evolution strategies (ES). Although FEM is widely used in many acoustic analyses, let us note that the boundary element method (BEM) is a more efficient numerical tool to model the interaction between the boundary parameters and the interior sound field. Furthermore, in virtue of the linear equations derived from the BEM formulation and the prior knowledge of the geometric segmentation of the surfaces, it is possible to derive an iterative algorithm that estimates the acoustic impedances of the surfaces. Let us remark also that, while numerical examples are shown in [10], an experimental setup in a controlled environment together with preliminary results are presented in further sections of this paper.

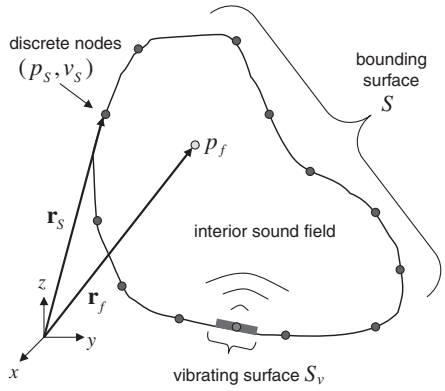

Fig. 1 Boundary element formulation of the interior sound field.

2. THEORETICAL FRAMEWORK

2.1. The Boundary Element Formulation of the Interior Field

Consider a sound field bounded by an arbitrary surface S where a subsegment S_v is harmonically vibrating at a frequency ω and radiating sound into the interior field, as depicted in Fig. 1. The boundary conditions at the nodal points $\boldsymbol{r}_S$ on S, namely the sound pressure p_S and the particle velocity v_S, are related to the sound pressure p_f at any point $\boldsymbol{r}_f$ in the interior by the Kirchhoff-Helmholtz integral equation

$$\oint_S \left(p_S \frac{\partial G(\boldsymbol{r}_S, \boldsymbol{r}_f)}{\partial \boldsymbol{n}} + j\omega\rho G(\boldsymbol{r}_S, \boldsymbol{r}_f)\, v_S \right) dS + p_f = 0, \quad (1)$$

where $G(\boldsymbol{r}_S, \boldsymbol{r}_f)$ denotes the three dimensional Green's function $G = e^{-jkr}/4\pi r$, with $r = |\boldsymbol{r}_S - \boldsymbol{r}_f|$, k the wave number, ρ the density of the field, and $j = \sqrt{-1}$.

Note in Eq. (1) that prescribing boundary values to p_S and v_S, the sound field p_f can be readily predicted (the forward analysis). However, in the inverse problem, both p_S and v_S are unknown, and the sound pressure p_f at different points represents input data directly measured from the test field. Therefore, if p_f is measured at M positions, and S is discretized into N nodes, a linear system of equations can be stated in a matrix equation using the discrete form of Eq. (1) [11], as follows:

$$\boldsymbol{A}_f\, \boldsymbol{p}_S - \boldsymbol{B}_f\, \boldsymbol{v}_S = -\boldsymbol{p}_f. \quad (2)$$

When constant elements on S and one node in their centroid is considered, the entries of the matrices $\boldsymbol{A}_f$ and $\boldsymbol{B}_f$ can be computed by the operators

$$\begin{aligned} a_{i,k} &= \oint_{S_k} \frac{\partial G(\boldsymbol{r}_k, \boldsymbol{r}_i)}{\partial \boldsymbol{n}}\, ds, \\ b_{i,k} &= -j\omega\rho \oint_{S_k} G(\boldsymbol{r}_k, \boldsymbol{r}_i)\, ds, \end{aligned} \quad (3)$$

with $i = 1, 2, \ldots, M$ and $k = 1, 2, \ldots, N$. In a similar way, if the points $\boldsymbol{r}_f$ are chosen to match the surface nodes, the following linear system is derived:

$$\boldsymbol{A}_S \boldsymbol{p}_S - \boldsymbol{B}_S \boldsymbol{v}_S = 0. \tag{4}$$

Furthermore, since the vibration strength of the sound source is assumed to be known, the corresponding nodal values become input data and Eq. (2) can be rewritten as

$$\boldsymbol{A}_f \boldsymbol{p}_S - \widetilde{\boldsymbol{B}}_f \widetilde{\boldsymbol{v}}_S = \widehat{\mathbf{B}}_f \widehat{\mathbf{v}}_S - \mathbf{p}_f, \tag{5}$$

denoting by $\widehat{\boldsymbol{v}}_S$ and $\widehat{\boldsymbol{B}}_f$ the known nodal particle velocities and their corresponding influence coefficients, and by $\widetilde{\boldsymbol{v}}_S$ the unknowns with their corresponding known influence coefficients $\widetilde{\boldsymbol{B}}_f$. Equation (5) describes the relationship between all the elements of the acoustic system: the sound source, the boundary S, and the interior field.

2.2. Statement of the Problem

Let us suppose that in a given room the acoustic impedances of the interior surfaces $S_1, S_2, \ldots, S_n$ are to be estimated. Assume also that one harmonic sound source (a speaker) produces a steady-state field in which the complex sound pressure at M arbitrary points is measured using a microphone, as illustrated in Fig. 2. The acoustic impedance z_S at any point x on the surfaces is given by the relation:

$$z_{S_x} = \frac{p_{S_x}}{v_{S_x}}. \tag{6}$$

Noting that the following are known parameters: 1) the geometry of the room, 2) information of the sound source (i.e. its location, vibration strength, phase and frequency), and 3) a set of sound pressures measured at M random points in the field, then the task is to recover the impedance values of the interior surfaces as defined by Eq. (6).

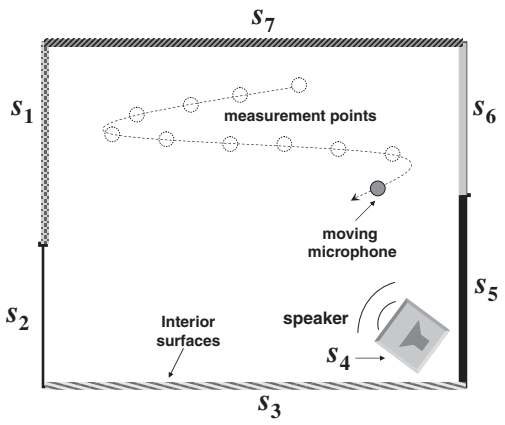

Fig. 2 Inverse estimation of the acoustic impedances on the surfaces of a room.

2.3. Estimation of the Acoustic Impedances: The T-SVD Based Approach

In inverse acoustics, a widely used approach to recover the p_S and v_S is based on singular value decomposition (SVD) analysis. This method consists on solving the BEM equations for one unknown boundary parameter at a time. In addition, truncation of some singular values (known as truncated-SVD or T-SVD [8,12,13],) is done to reduce the sensitivity to noise. This approach is briefly discussed here for the purpose of comparisons in further numerical examples.

First, let us observe that equations (2) and (4) form a linear system of two equations with two unknowns, hence they can be combined to solve for one unknown, for example $\boldsymbol{v}_S$, yielding

$$\boldsymbol{D}\, \boldsymbol{v}_S = \boldsymbol{p}, \tag{7}$$

where $\boldsymbol{D} = (\boldsymbol{A}_f \boldsymbol{A}_S^{-1} \boldsymbol{B}_S - \boldsymbol{B}_f)$ and $\boldsymbol{p} = -\boldsymbol{p}_f$. Notice that the degrees of freedom (DOF) of Eq. (7) is therefore $O(N)$. Because the matrix $\boldsymbol{D}$ is usually rank-deficient, Eq. (7) has to be solved in the least-squares sense using regularization techniques such as truncated-SVD analysis as follows.

Let $\boldsymbol{D} = \boldsymbol{U}\boldsymbol{\Sigma}\boldsymbol{W}^{\mathrm{H}}$ be the singular value factorization of $\boldsymbol{D}$, such that $\boldsymbol{U}\boldsymbol{U}^{\mathrm{T}} = \boldsymbol{W}\boldsymbol{W}^{\mathrm{T}} = \boldsymbol{I}$, $\mathrm{diag}(\boldsymbol{\Sigma}) = \{\alpha_1 \geq \alpha_2 \geq \ldots \geq \alpha_N\}$ are the singular values of $\boldsymbol{D}$, and the superscripts $^{\mathrm{H}}$ and $^{\mathrm{T}}$ are the hermitian and transpose respectively. The matrix $\boldsymbol{D}$ can be further represented as

$$\boldsymbol{D} = \boldsymbol{U}\boldsymbol{\Sigma}\boldsymbol{W}^{\mathrm{H}} = \sum_{i=1}^{N} \boldsymbol{u}_i \alpha_i \boldsymbol{w}_i^{\mathrm{H}}, \tag{8}$$

in which $\boldsymbol{u}_i$ and $\boldsymbol{w}_i$ are the left and right singular vectors respectively. Using the orthonormal properties of $\boldsymbol{U}$ and $\boldsymbol{W}$, the solution of Eq. (7) for $\boldsymbol{v}_S$ takes the form

$$\boldsymbol{v}_S = \boldsymbol{W}\boldsymbol{\Sigma}^{-1}\boldsymbol{U}^{\mathrm{H}}\boldsymbol{p}_f = \sum_{i=1}^{N} \frac{\boldsymbol{u}_i^{\mathrm{H}}\boldsymbol{p}_f}{\alpha_i}\, \boldsymbol{w}_i. \tag{9}$$

From Eq. (9) note that the effect of the singular values α_i's over $\boldsymbol{p}_f$ is an scaling factor. In practice, when the measurements of p_f are taken on the surface matching the nodal points, as in Fig. 3a, the computation of the influence matrices $\boldsymbol{A}$'s and $\boldsymbol{B}$'s of Eqs. (2) and (4) produces a full-rank $\boldsymbol{D}$ matrix in Eq. (7), but as soon as the measurements points are placed in the interior field (out of the surface, as in Fig. 3b), some rows of $\boldsymbol{D}$ tend to become linearly dependent making $\boldsymbol{D}$ rank-deficient. This effect is observed as a rapid decay of the singular values α_i's into small values (Fig. 3c, dotted line), which in turn makes the system sensitive to perturbations in p_f by amplifying the noise components. Therefore, in order to reduce the sensitiveness to noise, the regularization by truncation consists on discarding an appropriate number $(N - \lambda)$ of the smallest singular values. Thus, the solution of Eq. (7) becomes

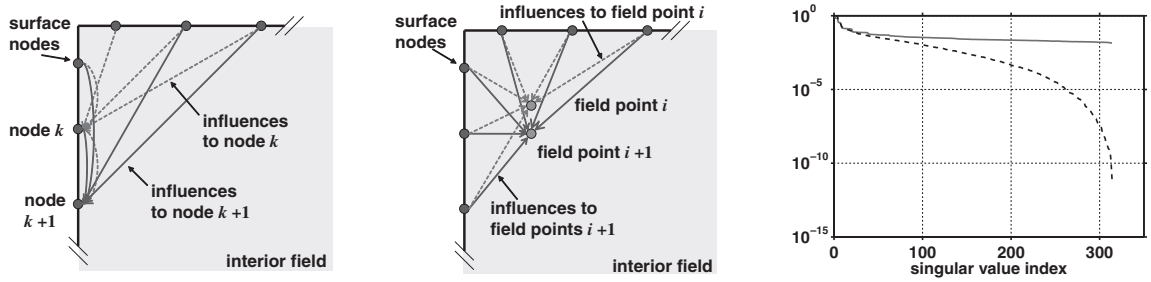

Fig. 3 a) Measurements taken at the surface nodal points. b) Measurements taken in the interior field. c) Example of singular values α_i of the matrix $\boldsymbol{D}$ when the measurements are taken at the surface nodal points (solid line), and when taken in the interior field (dotted line).

$$\boldsymbol{v}_{S_{T\text{-}SVD}} = \sum_{i=1}^{\lambda} \frac{\boldsymbol{u}_i^{\mathrm{H}} \boldsymbol{p}_f}{\alpha_i} \boldsymbol{w}_i = \boldsymbol{D}^{+} \boldsymbol{p}_f, \tag{10}$$

where $\boldsymbol{D}^{+}$ is the so-called pseudo-inverse of $\boldsymbol{D}$. Several criteria for the choice of the truncation number λ have been suggested in the literature, and a detailed description of some of them can be found in [14].

Once $\boldsymbol{v}_S$ is known, back substitution in Eqs. (2) and (4) yields the solution of $\boldsymbol{p}_S$, and the normal acoustic impedance at each node can be computed as in Eq. (6).

2.4. Iterative Estimation of the Acoustic Impedances

A drawback of the T-SVD approach is its high sensitivity to noise. Experience of previous work (e.g. [9,12,13]) has shown also that the estimation of $\boldsymbol{v}_S$ and $\boldsymbol{p}_S$ by this method tends to become more unstable as the DOF (i.e. the number of surface nodes) increases. On the other hand, it is possible to estimate the acoustic impedances of the surfaces in a more straightforward way and with reduced DOF leading to an improvement of noise sensitivity.

For simplicity, let us consider the geometry model of an empty room in which the surfaces have been clustered in such a way that each surface is define by a single homogeneous material (for example, information of appearance such as texture and color can be used to infer homogeneous regions), resulting in a total of n different surfaces $\{S_i | S = S_1 \cup S_2 \ldots S_n, \forall i = 1, 2, \ldots, n\}$, as illustrated in Figure 2. Thus, recalling the BEM formulation given in a previous section, two matrix equations can be derived by including the effect of the acoustic impedance z_S of the surfaces into Eqs. (4) and (5):

$$(\boldsymbol{C}_S - \tilde{\boldsymbol{B}}_S)\tilde{\boldsymbol{v}}_S = \hat{\boldsymbol{B}}_S \hat{\boldsymbol{v}}_S, \tag{11}$$

and

$$(\boldsymbol{C}_f - \tilde{\boldsymbol{B}}_f)\tilde{\boldsymbol{v}}_S = \hat{\boldsymbol{B}}_f \hat{\boldsymbol{v}}_S - \boldsymbol{p}_f, \tag{12}$$

where the elements of $\boldsymbol{C}_S$ and $\boldsymbol{C}_f$ are computed as

$$c_{i,k} = z_{S,k} \cdot a_{i,k}. \tag{13}$$

Let us further assume that each $z_{S,k}$ is basically determined by the local reaction at the incident point, (i.e. locally reactive surfaces), then, because the surfaces have been segmented by homogeneity, the following approximation holds:

$$\frac{p_{S_i,1}}{v_{S_i,1}} \approx \frac{p_{S_i,2}}{v_{S_i,2}} \approx \ldots \approx \frac{p_{S_i,m_i}}{v_{S_i,m_i}}, \tag{14}$$

or

$$z_{S_i,1} \approx z_{S_i,2} \approx \ldots \approx z_{S_i,m_i} = Z_i, \tag{15}$$

where m_i indicates the number of discrete nodes that belong to the i-th surface. Therefore, the original problem turns into that of finding the parameters Z_i's of the n surfaces.

Following the definition of the coefficients $c_{i,k}$ in Eq. (13), the nodal impedances can be grouped in accordance to Eq. (15), and Eq. (12) is rewritten in the matrix form of Eq. (16) in which the $a_{f,(i,k)}$'s are the $a_{i,k}$ elements of $\boldsymbol{A}_f$.

$$\begin{pmatrix} \sum_{k=1}^{m_1} a_{f,(1,k)}\,\tilde{v}_{S,k} & \sum_{k=m_1+1}^{m_2} a_{f,(1,k)}\,\tilde{v}_{S,k} & \cdots & \sum_{k=m_{n-1}+1}^{m_n} a_{f,(1,k)}\,\tilde{v}_{S,k} \\ \vdots & \vdots & \cdots & \vdots \\ \vdots & \vdots & \cdots & \vdots \\ \sum_{k=1}^{m_1} a_{f,(M,k)}\,\tilde{v}_{S,k} & \sum_{k=m_1+1}^{m_2} a_{f,(M,k)}\,\tilde{v}_{S,k} & \cdots & \sum_{k=m_{n-1}+1}^{m_n} a_{f,(M,k)}\,\tilde{v}_{S,k} \end{pmatrix} \begin{pmatrix} Z_1 \\ Z_2 \\ \vdots \\ Z_n \end{pmatrix} - \tilde{\boldsymbol{B}}_f \tilde{\boldsymbol{v}}_S = \hat{\boldsymbol{B}}_f \hat{\boldsymbol{v}}_S - \boldsymbol{p}_f \tag{16}$$

Writing Eq. (16) in a compact form yields

$$\langle \boldsymbol{A}_f \cdot \tilde{\boldsymbol{v}}_S \rangle \boldsymbol{z} - \tilde{\boldsymbol{B}}_f \tilde{\boldsymbol{v}}_S = \hat{\boldsymbol{p}}_f, \tag{17}$$

where $\langle \cdot \rangle$ indicates a column-grouped matrix, and $\hat{\boldsymbol{p}}_f = \hat{\boldsymbol{B}}_f \hat{\boldsymbol{v}}_S - \boldsymbol{p}_f$.

In Eq. (16) there are still two unknowns, namely the impedance values Z_i's and the nodal volume velocities $\tilde{\boldsymbol{v}}_S$, but in contrast to Eq. (7), an iterative optimization procedure can be now applied to find the desired surface impedances, as described in Algorithm 1 below.

At the first iteration ($l = 0$) of the procedure, the optimization is started with an initial guess of impedances $\boldsymbol{z}^{(0)} = \{Z_1^{(0)}, Z_2^{(0)}, \ldots, Z_n^{(0)}\}$. Afterwards, the process is continued until the evaluation of the objective function $f(\boldsymbol{p}_g, \boldsymbol{p}_f)$ satisfies the user-specified criterion ξ. Here $f(\boldsymbol{p}_g, \boldsymbol{p}_f)$ is defined as

$$f(\boldsymbol{p}_g, \boldsymbol{p}_f) = \frac{\|\boldsymbol{p}_g - \boldsymbol{p}_f\|^2}{\|\boldsymbol{p}_f\|^2} + \frac{1}{M-1} \frac{\|\boldsymbol{p}_G - \boldsymbol{p}_F\|^2}{\|\boldsymbol{p}_F\|^2}, \tag{18}$$

where $\boldsymbol{p}_g$ is a set of M sound pressures predicted at the same points of $\boldsymbol{p}_f$ using $\boldsymbol{z}^{(l+1)}$ through steps 4 and 5. The vectors $\boldsymbol{p}_G$ and $\boldsymbol{p}_F$ are respectively the sound pressures $\boldsymbol{p}_g$ and $\boldsymbol{p}_f$ taken in dB's.

The operator $\| \ \|$ indicates the euclidian norm.

At step 3 of the Algorithm 1, the update of $z^{(\ell+1)}$ involves a minimization problem (i.e. Eq. (19)) which is solved by nonlinear optimization using a Sequential Quadratic Programming (SQP) method. The implementation of this method is based on the algorithms described in [15,16], and is available as a function in the commercial software Matlab. Moreover, this function allows the user to input the bounds on the solution space indicated as $Z_{\min} \leq \boldsymbol{z} \leq Z_{\max}$. In practice, when the impedance of the materials is visualized in terms of the absorption coefficient α, positive values of the latter are expected. Hence, from the definition of the absorption coefficient

$$\alpha = 1 - \left| \frac{Z - \rho c}{Z + \rho c} \right|^2, \tag{22}$$

Algorithm 1: Iterative estimation of $\boldsymbol{z}$

1: Solve for $\tilde{\boldsymbol{v}}_S^{(l)}$ using $\boldsymbol{z}^{(0)}$ in Eq. (11)
2: While condition (21) is false do
3: Update $\boldsymbol{z}$ by
$$\boldsymbol{z}^{(l+1)} = \arg\min \|\langle \boldsymbol{A}_f \cdot \tilde{\boldsymbol{v}}_S^{(l)} \rangle \boldsymbol{z} - \tilde{\boldsymbol{B}}_f \tilde{\boldsymbol{v}}_S^{(l)} - \hat{\boldsymbol{p}}_f\| \quad \text{s.t. } Z_{\min} \leq \boldsymbol{z} \leq Z_{\max} \tag{19}$$
4: Update $\tilde{\boldsymbol{v}}_S^{(l+1)}$ using $\mathbf{z}^{(\ell+1)}$ in Eq. (11)
5: Compute $\boldsymbol{p}_g$ by
$$\boldsymbol{p}_g = \hat{\boldsymbol{B}}_f \hat{\boldsymbol{v}}_S - (\boldsymbol{C}_f - \tilde{\boldsymbol{B}}_f) \tilde{\boldsymbol{v}}_S^{(l+1)} \tag{20}$$
6: Evaluate
$$f(\boldsymbol{p}_g, \boldsymbol{p}_f) \leq \xi \tag{21}$$
7: $l \leftarrow l + 1$
8: end while

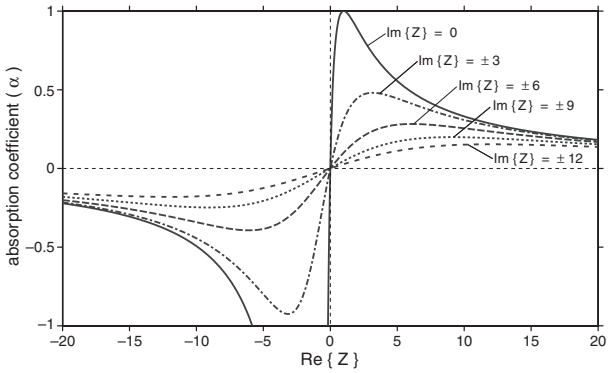

Fig. 4 Behaviour of the absorption coefficient in relation with the real and imaginary parts of the acoustic impedance.

and the observation of its general behavior with respect to the real and imaginary parts of Z (see Fig. 4), the bounds of the solution space are prescribed as $0 < \mathrm{Re}\{\boldsymbol{z}\} \leq Z_{\max}$ and $Z_{\min} \leq \mathrm{Im}\{\boldsymbol{z}\} \leq Z_{\max}$.

Let us further note that the DOF of the optimization problem (19) is n, i.e. the number of different surfaces in the room, while in the T-SVD based approach discussed before, the DOF is N (where $n \ll N$). Dealing with the inverse of a rank-deficient matrix is also avoided in the iterative approach by solving instead the optimization problem of Eq. (19). These makes the algorithm less sensitive to noise and allows us to place the measurement points at arbitrary locations in the interior field giving meaningful results after the analysis, as will be shown in the following numerical simulations.

3. NUMERICAL EXAMPLE

The geometry chosen for a numerical example is the 3D model of a realistic office room, which is shown in Fig. 5.

For a BEM analysis, the model is meshed using $N =$ 1,044 triangular-isoparametric elements with a maximum edge size of 0.24 m, allowing a frequency analysis up to 125 Hz (i.e. six elements per wavelength). The simulation test consists on recovering the acoustic impedance values of the interior surfaces from M field measurements simulated at uniformly distributed points in the field, using both the T-SVD and the iterative approaches. In the forward analysis, the set of M field pressures $\boldsymbol{p}_f$ is generated by manually assigning surface impedances relative to the impedance of the propagation media ($Z_0 = \rho c$). Table 1 shows the assessment of the surface impedances whose values have been arbitrarily assigned only with real part for simplicity. Once $\boldsymbol{p}_f$ is computed, the effect of the noise in the measurements is artificially simulated by adding broadband noise with a given signal to noise ratio (SNR) as follows:

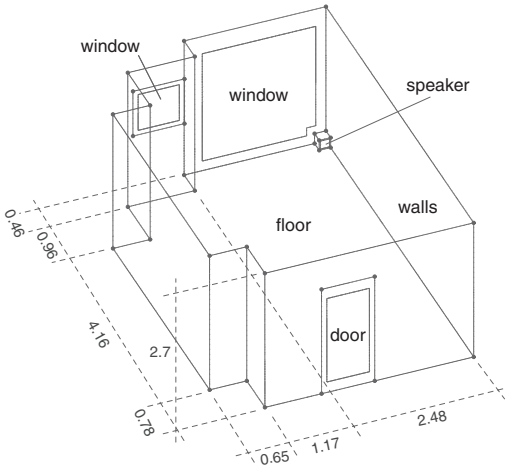

Fig. 5 3D geometry of an office (units in meters).

Table 1 Assignment of impedance values for the numerical example.

Surface	**Relative Impedance** ($Z = Z_c/Z_0$) (air: $Z_0 \approx 415$ Rayls)
Floor	37.0
Ceiling	260.0
Walls	55.0
Windows	108.0
Door	63.0

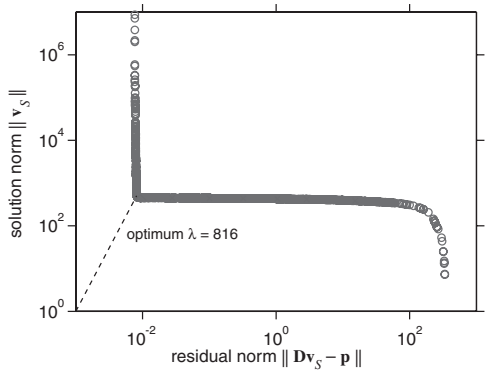

Fig. 6 Example of an L-cure showing the optimum value of λ for the T-SVD approach.

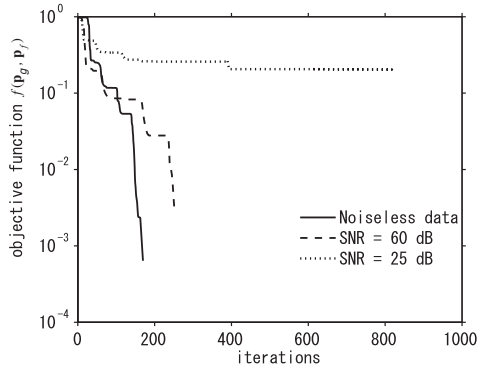

Fig. 7 Convergence history of the iterative approach in the numerical tests.

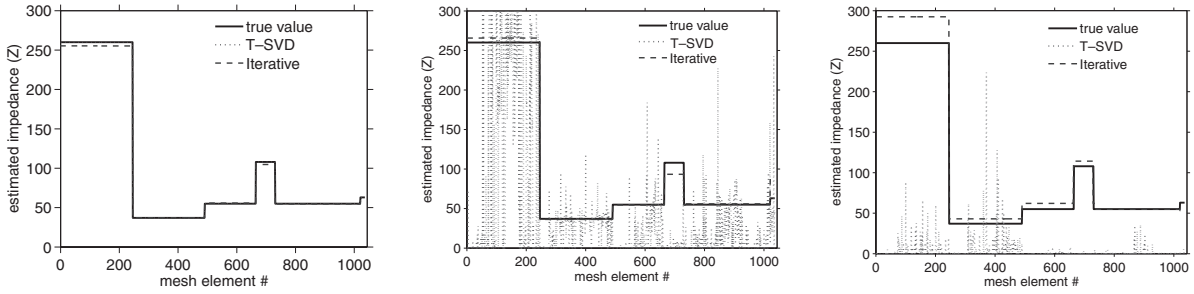

a) Noiseless b) SNR = 60 dB c) SNR = 25 dB

Fig. 8 Results obtained from the numerical tests at 125 Hz: impedance values recovered using the least-squares approach (T-SVD) with $M = 2N$ field pressures, and using the iterative optimization (Algorithm 1) with $M = N$ field pressures.

$$\boldsymbol{e} = (2\boldsymbol{\eta} - 1) \cdot \frac{\|\boldsymbol{p}_f\|}{\|\boldsymbol{\eta}\|} \cdot 10^{-\mathrm{SNR}/10},$$

$$\boldsymbol{p}_\mathrm{e} = \boldsymbol{p}_f + \boldsymbol{e}, \tag{23}$$

where $\boldsymbol{\eta}$ is an M-length vector whose elements are uniformly distributed within the interval $(\mathbf{0}, \mathbf{1})$. Thus, $\boldsymbol{p}_\mathrm{e}$ represents the simulated measurements.

In the case of the T-SVD analysis, the value of λ is computed using the L-curve approach [14]. Figure 6 shows an example of the optimum value of λ in the L-curve plot. For the optimization step of the iterative approach (step 3 of Algorithm 1), the solution space is constrained to $(Z_{\min} = -500) \leq \boldsymbol{z} \leq (Z_{\max} = 500)$, and the initial guess is set to $\boldsymbol{z}^{(0)} = \mathbf{1}$ (i.e. the relative acoustic impedance of the propagation media).

The performance of the iterative algorithm is illustrated in Fig. 7. The results of this numerical example are shown in Fig. 8 for the cases when SNR = {∞ dB (noiseless), 60 dB, 25 dB}. From these results it can be observed that both methods successfully recovered the surface impedances when the measurements are free from noise. However, when noise is attached to the data, the accuracy of the

T-SVD approach is greatly degenerated (as seen in Fig. 8c), while the iterative approach converged, in the worst case, to a value of 0.42 (in a normalized scale) and still giving meaningful impedance values. On the other hand, the selection of an appropriate threshold ξ is crucial. If too small values of ξ are chosen, the condition of Eq. (21) is frequently not satisfied and the process has to be stopped before the solutions at each iteration start to fit the noise in the data. For this numerical example, ξ has been assign as small as 1×10^{-2} which was successfully satisfied for the cases of SNR = {noiseless, 60 dB} (see Fig. 7). The process was prematurely stopped for the case of SNR = 25 dB. While the parameter ξ, together with a minimum-improvement threshold, has been used to stop the iterations in the current implementation, a universally applicable stopping criterion is still a subject of research.

In general, the iterative approach was proved to be robust to noise and therefore suitable for practical applications. For this reason, only the iterative method will be further considered for experimental tests.

4. EXPERIMENTAL SETUP

Preliminary experiments consisted on attempting to estimate the acoustic impedance of the interior surfaces of a 30 mm thick-acrylic reverberation chamber whose dimensions are shown in the diagram of Fig. 9. In this chamber, different types of surfaces were setup by installing three commonly used acoustic absorbents: glass wool 50 mm $-$ 32 kg/m^3, glass wool 15 mm $-$ 32 kg/m^3, and wool felt 5 mm $-$ 96 kg/m^3. Figure 10a shows the location of these test surfaces.

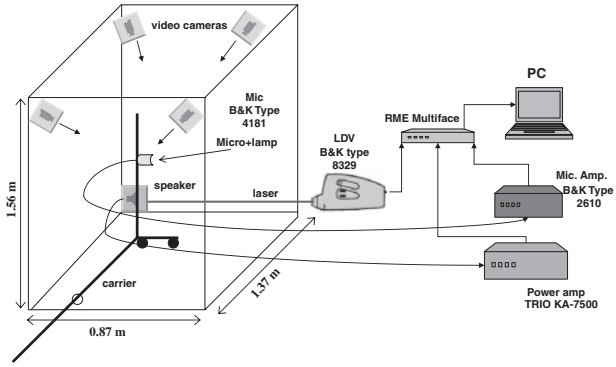

Fig. 9 Artifacts used for the experiments.

The physical parameters to be measured during the experiments are the vibration velocity of the sound source and M sound pressures (amplitude and phase) which are expressed respectively as follows:

$$v_{\text{source}} = |V|e^{j(\omega t+\theta_v)},$$
$$p_f = |P|e^{j(\omega t+\theta_f)}. \tag{24}$$

For a steady state analysis the time factor can be omitted. If in addition the phase of the source signal is $\theta_v = 0$, then the amplitude $|V|$ is directly observed from the Laser Doppler Vibrometer (LDV). $|P|$ and the phase θ_f are obtained from the microphone and the LDV signals.

In the data analysis stage, the 3D coordinates of the measurements must be known. Thus, the location of the microphone at the time of recording each sound sample is estimated in real-time by 3D stereoscopic-tracking employing the four overhead video cameras. These cameras are

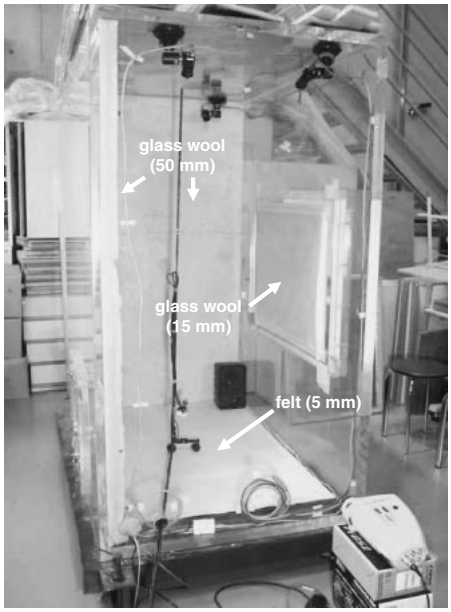

a)

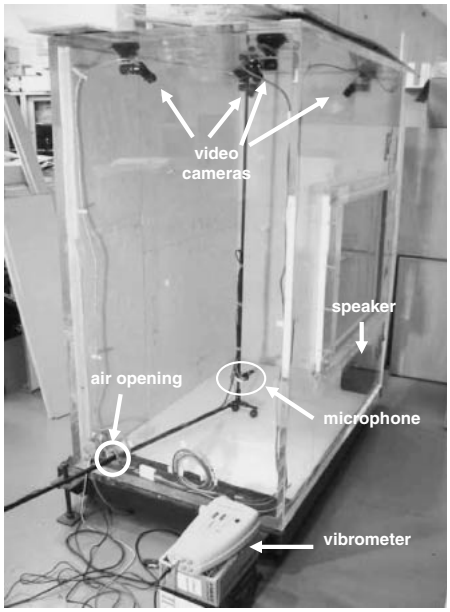

b)

Fig. 10 a) Test surfaces considered for the experiments. b) Actual setup of the devices in the experimental chamber.

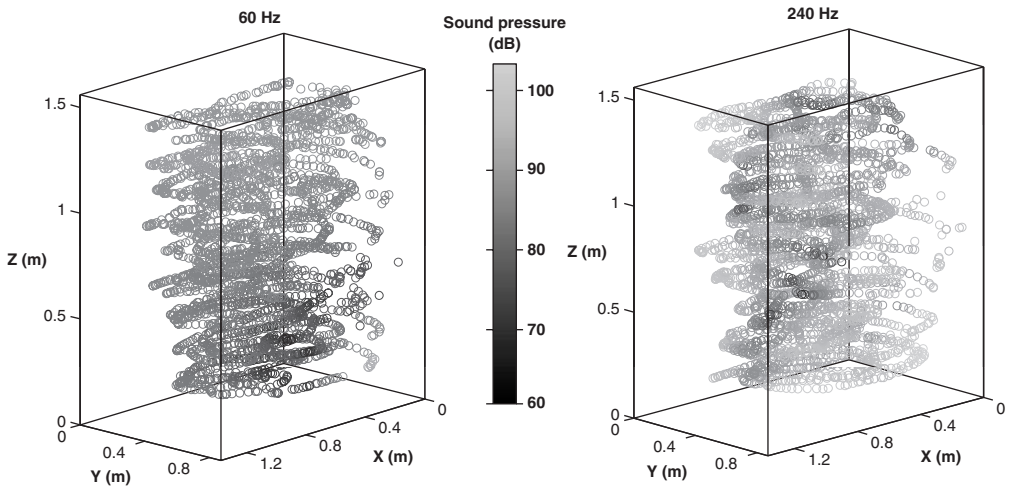

Fig. 11 Example of 3D points and field pressures measured in the experiments with absorbent materials at 60 Hz and 240 Hz.

easily mounted in the interior of the chamber, and their size ($3 \times 3 \times 5$ cm) is comparably smaller than the analysis wavelengths allowing us to neglect their acoustic scattering effect.

Although the microphone can be freely moved in the interior space while the speaker is emitting a tone, the speed μ (in m/s) at which the microphone can be displaced is constrained by the frequency f_s of the tone, otherwise the doppler effect will introduce inaccurate measurements. Hence, from the doppler relation formula, μ is given by

$$\mu \leq c\left(\frac{f_s + |\beta|}{f_s} - 1\right), \tag{25}$$

where c is the velocity of sound in the medium, and β is the tolerated frequency deviation (in Hz) of the signal observed at the microphone. The frequency range for the experiments is 60 Hz to 240 Hz with steps of 20 Hz. At each analysis frequency, $M = 2N$ sound pressures were measured in the interior field.

For the BEM analysis of the experimental data, the chamber is modeled with a mesh of 1446 triangular-isoparametric elements. The model of the homogenous surfaces in the interior are defined as it is shown in Fig. 10a: surface type #1) two lateral walls covered with the 50 mm glass wool, surface type #2) the floor covered with the 5 mm felt, and surface type #3) a rectangle area on a lateral wall covered with the 5 mm glass wool. The bare walls and ceiling of the chamber are considered as rigid boundaries in the model.

When performing the experiments, the carrier that holds the microphone (see Fig. 10b) allows displacement only in the horizontal plane. Therefore, the M measurements are distributed in planes with equidistant hight. Figure 11 shows two examples of the sound pressures acquired by the implemented measurement system.

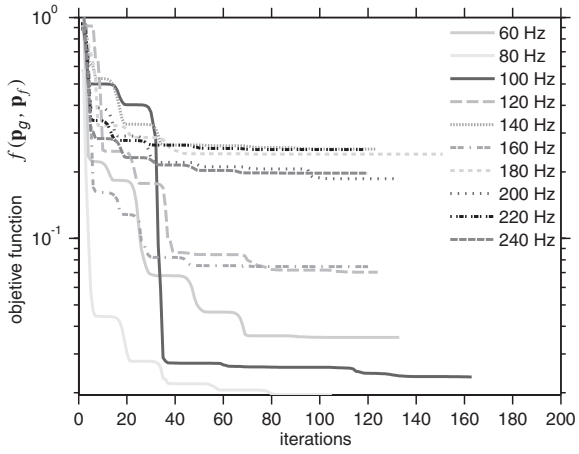

Fig. 12 Convergence history of the iterative estimation of the surface impedances using experimental data.

5. EXPERIMENTAL RESULTS

To start the iterations of the Algorithm 1, the initial guess was set to $\boldsymbol{z}^{(0)} = \mathbf{1}$. Furthermore, the unknown surface impedances were assumed to lie within the normalized bounds $0 < \mathrm{Re}\{z\} < 1{,}000$ and $-1{,}000 < \mathrm{Im}\{z\} < 1{,}000$. Using these initialization settings, the iterative process performed as shown in Fig. 12. Lets us note first that in none of the analysis the specified stopping threshold $\xi = 0.01$ (or 1%, in the percent of the normalized range) was achieved. The closest was 0.017 for the case of 80 Hz. Nevertheless, the algorithm converged to the experimental results that are shown in Fig. 13 where the real and imaginary part of the normalized acoustic impedance is plotted for each test material. These impedances are further visualized in terms of the absorption coefficients in Fig. 14.

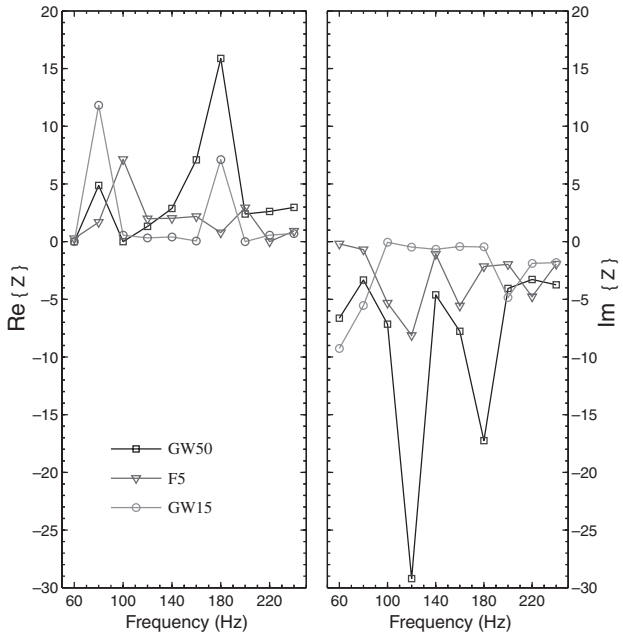

Fig. 13 Normalized impedances recovered by the iterative Algorithm 1 using the experimental data. Glass wool 50 mm (GW50), wool felt 5 mm (F5), glass wool 15 mm (GW15).

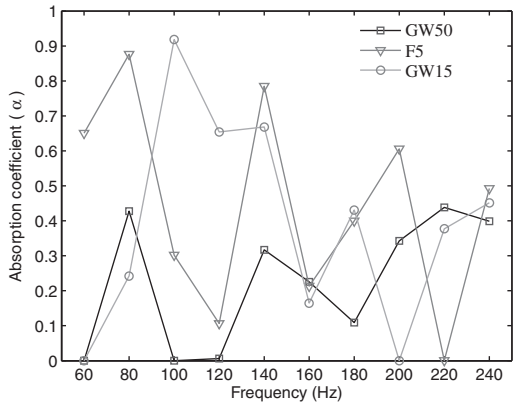

Fig. 14 Absorption coefficients computed from the experimental results. Glass wool 50 mm (GW50), wool felt 5 mm (F5), glass wool 15 mm (GW15).

During the analysis of the experimental data, the iterative process (Algorithm 1) has been run with four different subsets of $M = N$ arbitrary measurements out of the total $M = 2N$ acquired. Thus for each frequency, the mean and standard deviation of the error between the predicted and actual sound field in dB's $|\boldsymbol{p}_G - \boldsymbol{p}_F|$ has been plotted in Fig. 15. The validation of experimental results is often done by comparisons with the ground-truth data or with results obtained by other measurement methods. However, by the time of preparation of this material, there is still no other practical method to estimate the acoustic impedances of the surfaces under similar conditions (i.e. in an enclosed space with different types of materials

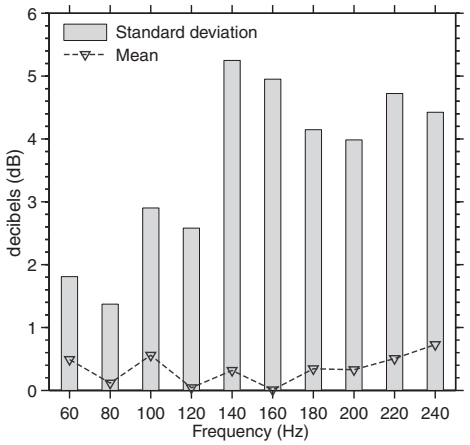

Fig. 15 Standard deviation and mean of the error $|\boldsymbol{p}_G - \boldsymbol{p}_F|$.

interacting with each other). Therefore, this lack of true data impedes an immediate validation of the method, but in the other hand, the rates of Fig. 15 can give margins of the expected error within the specified frequency when numerical simulations with the model of the chamber and the tested materials are performed. As Fig. 15 suggests, the estimated acoustic impedances approximate the actual sound field within a maximum average error of 0.7 dB's (for 240 Hz), and in the worst case, with a standard deviation of 5.2 dB's (for 140 Hz).

6. CONCLUSIONS

Two theoretical frameworks for the estimation of acoustic impedance on the surfaces of interiors have been compared with numerical examples: on one hand, a method based on the traditional T-SVD analysis, and on the other hand, a novel iterative approach based on the boundary element method. The latter was further tested with experiments in a controlled environment. The preliminary results suggest that indeed, it is possible to get an estimate of the normal-incidence acoustic impedances of the test materials by using the inverse formulation of the BEM and prior knowledge of the geometry of the surfaces. Approaching the problem in this way (together with the measurement system implemented) overcomes most of the physical constraints that traditional methods suffer. A key point to keep in mind, however, is that because of the inherent features of its framework, the system considers only the local impedance effect (local reaction) of the surfaces. If surfaces with extended reaction are present (e.g. those of thick-porous objects), a suitable model (e.g. FEM) should be included for those surfaces in the general BEM analysis. Improvements can also be achieved in the measurement process. In the current implementation, the measurements must be repeated for each analysis frequency outputting a pure tone from the speaker. This troublesome process can be avoided by using broadband noise and careful Fourier

analysis of the data, thus the acoustic impedance for a range of frequencies can be computed. Other improvements are in the computational cost. Because the system requires the storage of two N^2 and two $M \times N$ complex full-populated matrices, the immediate use of the iterative method in a real-scale room is still prohibited. Nevertheless, note that this method requires only the computation of the objective function Eq. (18) and the evaluation of Eq. (21), hence the possibility to use highly efficient BEM implementations that do not require full matrix storage. Among the candidates to exploit this feature is the Fast Multipole BEM (FMBEM) which has been successfully used for the acoustic analysis of large-scale models [17].

REFERENCES

[1] C. Noke and V. Mellert, "Breif review on *in situ* measurement techniques of impedance or absorption," in *Proc. Forum Acusticum*, Sevilla (2002).

[2] J. F. Allard, C. Depoiller and P. Guignouard, "Free field surface impedance measurements of sound absorbing materials with surface coatings," *Appl. Acoust.*, **26**, 199–207 (1989).

[3] A. J. Cramond and C. G. Don, "Reflection of impulses as a method of determining the acoustic impedance," *J. Acoust. Soc. Am.*, **75**, 328–344 (1984).

[4] E. Mommertz, "Angle-dependent *in situ* measurement of reflections coefficients using a substraction technique," *Appl. Acoust.*, **46**, 251–264 (1995).

[5] R. Lanoye, G. Vermeir and W. Lauriks, "Measuring the free field acoustic impedance and absorption of sound absorbing materials with a combined particle velocity-pressure sensor," *J. Acoust. Soc. Am.*, **119**, 2826–2831 (2006).

[6] Y. Takahashi, T. Otsuru and R. Tomiku, "*In situ* measurements of surface impedance and absorption coefficients of porous materials using two microphones and ambient noise," *Appl. Acoust.*, **66**, 845–865 (2005).

[7] J. D. Maynard, E. G. Williams and Y. Lee, "Nearfield Acoustic Holography: I. Theory of the generalized holography and the developement of the NAH," *J. Acoust. Soc. Am.*, **78**, 1395–1413 (1985).

[8] M. R. Bai, "Application of BEM (boundary element mehtod)-based acoustic holography to radiation analysis of sound sources with arbitrarily shaped geometries," *J. Acoust. Soc. Am.*, **92**, 533–549 (1992).

[9] E. G. Williams and B. H. Houston, "Interior near–field acoustical holography in flight," *J. Acoust. Soc. Am.*, **108**, 1451–1463 (2000).

[10] G. Dutilleux, F. C. Sgarg and U. R. Kristiansen, "Low-frequency assessment of the *in situ* acoustic absorption of materials in rooms: an inverse problem approach using evolutionary optimization," *Int. J. Numer. Methods Eng.*, **53**, 2143–2161 (2002).

[11] O. von Estorff, *Boundary Elements in Acoustics—Advances and Applications* (WIT Press, Southampton, UK, 2000).

[12] P. A. Nelson and S. H. Yoo, "Estimation of acoustic source strength by inverse methods: Part I, conditioning of the inverse problem," *J. Sound Vib.*, **233**, 643–668 (2000).

[13] B.-K. Kim and J.-G. Ih, "On the reconstruction of the vibro-acoustic field over the surface enclosing and interior space using the boundary element method," *J. Acoust. Soc. Am.*, **100**, 3003–3016 (1996).

[14] P. C. Hansen, "Regularization tools: A Matlab package for analysis and solution of discrete ill-posed problems," *J. Numer. Algorithms*, **6**, 1–35 (1994).

[15] S. P. Han, "A globally convergent method for nonlinear programming," *J. Optimization Theory Appl.*, **22**, 297 (1977).

[16] M. J. D. Powell, "A fast algorithm for nonlinearly constrained optimization calculations," in *Numerical Analysis*, Lecture Notes in Mathematics, 630 (Springer Verlag, Berlin, 1978).

[17] T. Sakuma and Y. Yasuda, "Fast Multipole Boundary Element Method for large-scale steady-state sound field analysis. Part I: setup and validation," *Acta Acustica united with Acustica*, **88**, 513–525 (2002).

Gabriel Pablo Nava completed his B.E. studies in Mexico City at the Instituto Politecnico Nacional in 1999. He received his M.S. and Ph.D. degrees in 2004 and 2007 respectively, from the Department of Information Science and Technology of the University of Tokyo. After staying as a postdoc at the Institute of Industrial Science of the University of Tokyo until March 2008, he joined the Innovative Communications group of the NTT Communication Science Laboratories where he is currently conducting research on acoustics for sound localization in the t-Room project.

Yosuke Yasuda graduated from the Faculty of Engineering of the University of Tokyo in 1999 and received a Ph. D. degree from the same university in 2004. He was a JSPS Research fellow at the Institute of Industrial Science of the University of Tokyo from 2004 to 2007. Research fellow of Department of Socio-cultural Environmental Studies, Graduate School of Frontier Sciences, University of Tokyo since 2007. Member of the Acoustical Society of Japan and the Architectural Institute of Japan. Excellent Master's Thesis Award from the Architectural Institute of Japan, 2001, and Awaya Prize from ASJ, 2005.

Yoichi Sato is an associate professor jointly affiliated with the Graduate School of Interdisciplinary Information Studies, and the Institute of Industrial Science, at the University of Tokyo, Japan. He received the BSE degree from the University of Tokyo in 1990, and the M.S. and Ph.D. degrees in robotics from the School of Computer Science, Carnegie Mellon University, Pittsburgh, Pennsylvania, in 1993 and 1997 respectively. His research interests include various topics in computer vision such as physics-based vision, reflectance analysis, image-based modeling and rendering, tracking and gesture analysis, and computer vision for HCI.

Shinichi Sakamoto received his B.S. in 1991 and his Ph.D. degree in 1996 from the Faculty of Engineering of the University of Tokyo. He is currently an Associate professor at the Institute of Industrial Science of the University of Tokyo where he conducts research on architectural acoustics and environmental noise control. Granted with the Awaya Prize from the Acoustic Society of Japan in 2001, and prized for outstanding presentations at the annual meetings of the INCE-Japan in 2001. Member of the Architectural Institute of Japan and ASJ.